Dyes and Pigments 183 (2020) 108712

Contents lists available at ScienceDirect

Dyes and Pigments

journal homepage: http://www.elsevier.com/locate/dyepig

Evaluation of asymmetric orthogonal cyanine fluorophores

Albertus W. Hensbergen [a], Mathijs A.C. de Kleer [a], Michael S. Boutkan [a], Danny M. van Willigen [a], Felicia A. van der Wijk [a], Mick M. Welling [a], Hans-Jürgen Wester [b], Tessa Buckle [a], Fijs W.B. van Leeuwen [a,*]

[a] Interventional Molecular Imaging Laboratory, Department of Radiology, Leiden University Medical Center, Albinusdreef 2, 2333, ZA, Leiden, the Netherlands
[b] Pharmazeutische Radiochemie, Technische Universität München, Walther-Meißner-Straße 3, 85748, Garching, Germany

ARTICLE INFO

Keywords:
Fluorescence
Cyanine fluorophores
Fluorescence brightness
Photobleaching
Image-guided surgery

ABSTRACT

Pentamethine cyanine (Cy5) fluorophores have proven to be versatile imaging agents (*i.e.*, tracers) for a range of micro- and macroscopic imaging applications, including image-guided surgery. In this study the relationship between the structure of asymmetric Cy5 fluorophores and their photophysical properties was studied. To this end, seven Cy5 analogues, bearing orthogonal *N*-indole substituents (H, SO_3^-, or benzene), were synthesised and evaluated. In-depth analysis revealed that introduction of sulfonates enhanced the fluorescence brightness and photostability, while reducing the lipophilicity, serum binding and stacking tendency. The addition of benzene moieties induced a bathochromic shift of 10–20 nm, increased the lipophilicity (LogP = -1.56–1.23) and serum binding (67.3–93.8% bound), as well as negatively impacted the brightness ($0.74–42.9 \cdot 10^3$ M^{-1} cm^{-1}), photostability (24.4–90.6% remaining), and stacking tendency. Chemical stability was uninfluenced by the substitution pattern. Additionally, the generation of a c[RGDyK]-based hybrid tracer based on one of these fluorophores in combination with a diethylenetriaminepentaacetic acid (DTPA) chelate and an ^{111}In-isotope was reported. This compound was evaluated *in vitro* using $\alpha_v\beta_3$-overexpressing Geβ3 cells and *in vivo* using a 4T1 mouse tumour model. Overall, the presented results imply that alterations of the asymmetrical orthogonal Cy5 fluorophore structure have impact on the (photo)physical properties. Furthermore, the orthogonal Cy5 fluorophore framework can readily be applied in tracer development.

1. Introduction

With the rise of fluorescence-guided surgery in oncology, the demand for specific and highly fluorescent tracers has grown substantially. Next to fluorophores such as indocyanine green and fluorescein being routinely used in clinical care [1,2], various ongoing clinical trials make use of investigative new imaging agents (*i.e.*, tracers) targeting receptors highly expressed on the membranes of tumorous cells [3–5]. Fluorophores from the cyanine (Cy) family are the most commonly used fluorophores in image-guided surgery [6]. The structure of the fluorophore also impacts the photophysical properties; the fluorescence quantum yield (Φ_F) of a fluorophore can be influenced by its substituents on either indole unit [7], but a clear trend between the substitution pattern on indoles and the Φ_F has not been found [8,9]. Ultimately, when conjugated to a targeting vector, the fluorophore structure can considerably influence the performance—*e.g.*, receptor affinity, pharmacodynamics and pharmacokinetics—of the corresponding tracer [10–13]. These effects have been studied using either near-infrared heptamethine (Cy7) [14,15] or far-red pentamethine (Cy5) analogues [11,16].

In addition to the fluorophore structure, the position where the fluorophore is incorporated in a (hybrid) tracer has also been shown to influence tracer performance [11]. Most fluorescent (and hybrid) tracers are based on an "end-labelled fluorophore" design, meaning that the targeting moiety is coupled to the fluorescent moiety without being integrally intertwined. Literature also indicates that shielding of the fluorophore could reduce the (possibly negative) influence(s) exerted by a fluorescent label [17]. This finding engendered the concept of using fluorophores as spacers during functionalization [18–20]. While literature mostly describes cyanine fluorophores containing symmetrical *N*-indole substituents to be used in tracer design, recent reports also mention asymmetrical orthogonal cyanine fluorophores [11,21,22].

The impact of the substituents of a fluorophore on tracer affinity, pharmacodynamics, and pharmacokinetics is well described [16,

* Corresponding author.
E-mail address: f.w.b.van_leeuwen@lumc.nl (F.W.B. van Leeuwen).

https://doi.org/10.1016/j.dyepig.2020.108712
Received 23 March 2020; Received in revised form 10 July 2020; Accepted 11 July 2020
Available online 6 August 2020

22–24]. For asymmetrical penta- and heptamethine cyanine fluorophores, the influence of small variations in these substituents (*e.g.*, a single sulfonate or benzene substituent at the (C4 and) C5 position of either indole) can exert on the lipophilicity, serum binding quantum yield, molar extinction coefficient, stacking behaviour, and chemical- and photostability has also been studied [9,13], as well as the influence of the polymethine bridge length on the signal penetration depth [25]. For asymmetrical orthogonal Cy5 fluorophores (*i.e.*, a cyanine fluorophore that bears a single sulfonate or benzene substituent at the (C4 and) C5 position of either indoles and has different *N*-indole substituents suited for conjugation) these features have, to the best of our knowledge, not yet been examined. Hence, in this study the characterisation of an asymmetrical orthogonal Cy5 framework (Phth-(R^1)Cy5(R^2)-COOH, where either or both R^1 and R^2 equal H, SO_3^-, or benzene (Scheme 1)) was evaluated. In addition, a novel c[RGDyK]-based hybrid tracer was created in order to study if asymmetrical orthogonal fluorophores have potential for angiogenesis imaging purposes by using c[RGDyK]; the latter is a proven model for evaluating tracer development strategies [22,26,27].

2. Materials & methods

2.1. Chemistry

2.1.1. General

All chemicals and solvents were obtained from commercial sources and used without further purification. Dimethylformamide (DMF), dichloromethane (DCM) and dimethylsulfoxide (DMSO) were dried with 4 Å molecular sieves, unless stated otherwise. Column chromatography was performed with 40–63 μm silica from Screening Devices (Amersfoort, The Netherlands). Dry column vacuum chromatography (DCVC) was performed as published by Pedersen *et al.* [28] with 15–40 μm silica

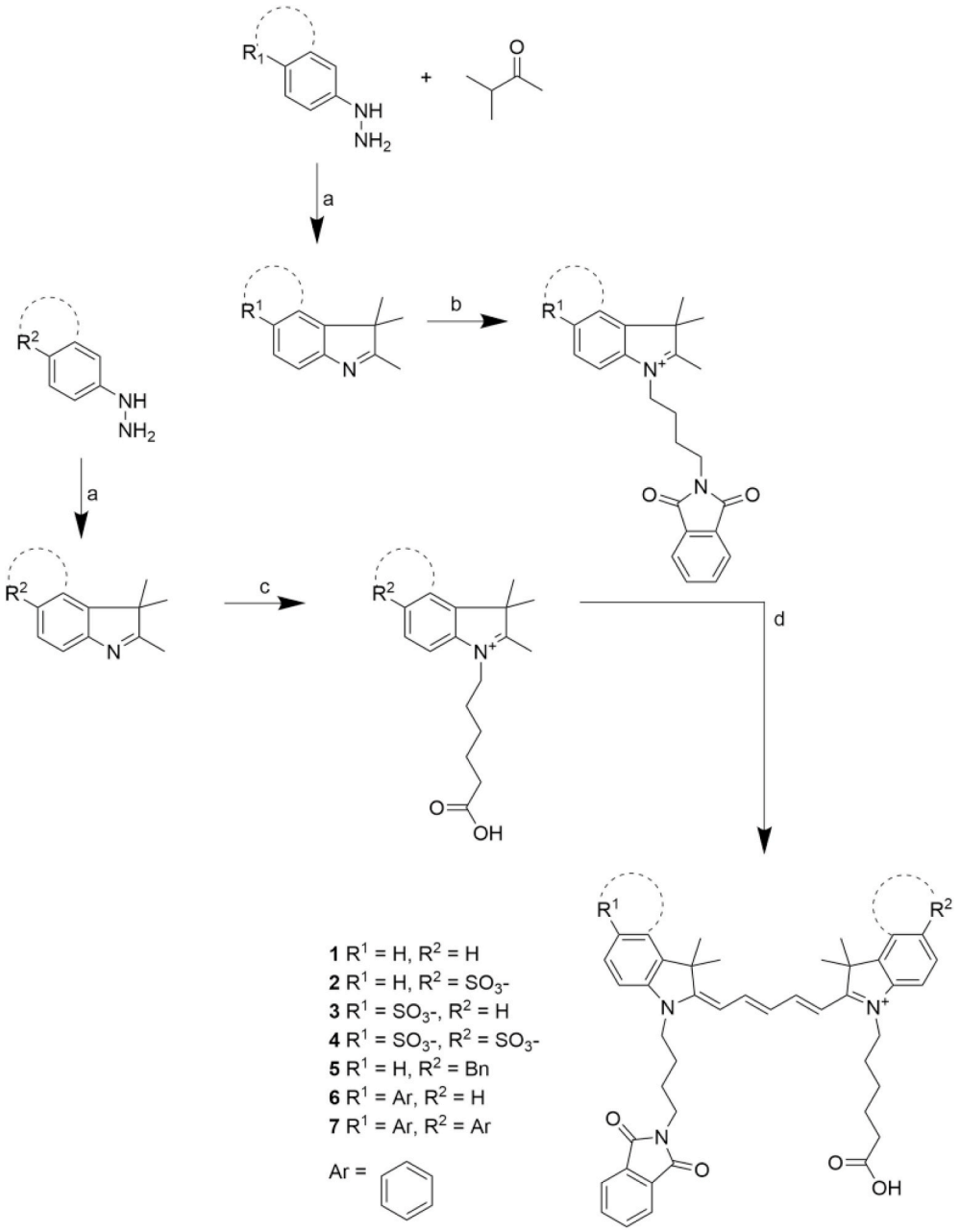

Scheme 1. Synthesis scheme for fluorophores **1**–**7**. a) AcOH, 90 °C, 24 h, b) 1-(4-bromobutyl)pyrrolidine-2,5-dione in sulfolane, 90 °C, 72 h, c) 6-bromohexanoic acid in 1,2-dichlorobenzene or acetonitrile, 95–120 °C, 72 h, d) AcOH/Ac_2O (1:1), 60–120 °C, 12 h; pyridine/Ac_2O (3:1), r.t., 12 h.

and Hyflo Supercell Celite (Fisher Scientific, Hampton, US). High-performance liquid chromatography (HPLC) was performed on a Waters HPLC system using either a 1525 EF or 2545 pump and a 2489 UV/VIS detector. For preparative HPLC either a Dr. Maisch GmbH Reprosil-Pur 120C18-AQ 10 μm (250 × 20 mm) column or a XBridge Prep C8 10 μm OBD 250 × 30 mm column was used with a gradient of 0.1% trifluoroacetic acid (TFA) in H_2O/acetonitrile (CH_3CN) 95:5 to 0.1% TFA in H_2O/CH_3CN 5:95 in 40 min (12 or 25 mL/min, respectively) was employed. For semi-preparative HPLC a Dr. Maisch GmbH Reprosil-Pur C18-AQ 10 μm (250 × 10 mm) column was used and a gradient of 0.1% TFA in H_2O/CH_3CN 95:5 to 0.1% TFA in H_2O/CH_3CN 5:95 in 40 min (5 mL/min) was employed. For analytical HPLC a Dr. Maisch GmbH Reprosil-Pur C18-AQ 5 μm (250 × 4.6 mm) column was used and a gradient of 0.1% TFA in H_2O/CH_3CN 95:5 to 0.1% TFA in H_2O/CH_3CN 5:95 in 40 min (1 mL/min) was employed. High-resolution mass spectrometry (HRMS) was performed on either on-line C18 nanoHPLC MS/MS with a system consisting of an Easy nLC 1200 gradient HPLC system (Thermo Fisher, Bremen, Germany), and a LUMOS mass spectrometer (Thermo Fisher, Bremen, Germany) with a gradient from of 0.1% formic acid (FA) in H_2O/CH_3CN 98:2 to 0.1% TFA in H_2O/CH_3CN 20:80 in 30 min, or a Waters Acquity H-class UPLC (Waters, Milford, USA) using a Acquity UPLC BEH C18 1.7 μm (2.1 × 50 mm) column with a gradient of 0.1% FA in H_2O/CH_3CN 98:2 to 0.1% FA in H_2O/CH_3CN 60:40 in 1.8 min (0.6 mL/min) coupled to a high-resolution XEVO G2S-XTOF Mass Spectrometer (Waters, Milford, USA). Low-resolution mass spectrometry (LRMS) was performed using a Bruker Microflex matrix-assisted laser desorption ionisation time-of-flight (MALDI-TOF) mass spectrometer. ^{1}H and ^{13}C NMR were performed on a Bruker AV-300 (300 MHz) or a Bruker Ascend 850 (850 MHz) equipped with a CryoProbe (all from Bruker, Billerica, United States) in deuterated solvents. Absorbance spectra were recorded using an Ultrospec 2100 pro (Amersham Biosciences, Little Chalfont, UK). Fluorescence spectra were recorded using a PerkinElmer LS-55 (PerkinElmer, Waltham, USA).

2.1.2. Synthesis

2.1.2.1. Merrifield resin synthesis. As performed by Lopalco *et al.* [29] Chloromethyl polystyrene resin (8.3 g, 15.0 mmol), *N-tert*-butoxycarbonyl-(*N*-Boc) aminophenol (9,4 g, 45.0 mmol), TBAI (1,7 g, 4.5 mmol) and Cs_2CO_3 (14.7 g, 45.0 mmol) were dissolved in acetone, refluxed at 70 °C overnight under nitrogen atmosphere. The resin was then washed extensively with 100 mL DMF, H_2O, DMF, DCM and diethyl ether (Et_2O) and dried *in vacuo*. A 4-(4-nitrobenzyl)pyridine test was used to determine reaction completion. 10.3 g (90% isolated yield) of Merrifield resin was formed. Removal of the *N*-Boc protection group was carried out by adding a solution of 20% TFA in DCM. After washing with DCM, the resin was neutralised using 20% *N,N*-diisopropylethylamine (DiPEA) in DCM and after washing with DCM the resin was used in further steps.

The 2,3,3-trimethyl-3*H*-indole-5-sulfonate- and 1,1,2-trimethyl-1*H*-benzo[*e*]indole-based precursors for the Cy5 fluorophores were synthesised as previously published [11,16,22] and used without further purification.

2.1.2.1.1. Synthesis of phthalimide fluorophores. The synthesis of **1**–**3**, **5**, and **6** has previously been described [11]. The following compounds were synthesised in a similar fashion, which is in short as follows: the hemicyanine was prepared by heating the indole-based building block with *N*-((1*E*,3*E*)-3-(phenylimino)prop-1-en-1-yl)aniline in a mixture of acetic acid/acetic anhydride (AcOH/Ac_2O; 1:1) to 90 °C for 18 h followed by stirring at 120 °C for 2 h. After full conversion of the starting material (as determined by using UV/Vis spectroscopy ($\lambda_{max,\ product} \approx 450$ nm, $\lambda_{max,\ starting\ material} \approx 390$ nm)), the mixture was cooled down to room temperature (r.t.) and precipitated in Et_2O. After repeated centrifugation, decanting and washing steps with Et_2O and ethyl acetate (EtOAc), the obtained solid was dissolved in a 1:1 DCM/DMF mixture and directly added to the deprotected resin. The suspension was agitated at r.t. for 60 min. Then, the resin was washed with DCM/DMF mixtures and the cyanine fluorophore was prepared by adding the corresponding second indole-based building block in a mixture of pyridine/Ac_2O (3:1). The resulting mixture was agitated at r.t. for 18 h. Crude compounds were purified by means of DCVC (EtOAc/MeOH) and subsequent preparative HPLC.

2.1.2.2. 1-(5-carboxypentyl)-2-((1E,3E)-5-((E)-1-(4-(1,3-dioxoisoindolin-2-yl)butyl)-3,3-dimethylindolin-2-ylidene)penta-1,3-dien-1-yl)-3,3-dimethyl-3H-indol-1-ium (1). As previously described [11]. ^{13}C NMR (850 MHz, CD_3OD δ 177.16, 169.86, 155.55, 155.50, 155.39, 143.47, 143.46, 142.65, 142.53, 135.41, 133.20, 129.75, 129.69, 126.67, 126.63, 126.58, 126.31, 126.16, 124.14, 123.41, 123.37, 112.07, 111.93, 104.44, 104.43, 104.33, 104.32, 50.58, 50.46, 44.81, 44.27, 38.11, 34.59, 31.13, 28.19, 27.92, 27.90, 27.33, 26.62, 25.69, 25.38. HRMS calculated $[M]^+$ for $C_{43}H_{48}N_3O_4^+$ 670.3639 found 670.3643.

2.1.2.3. 1-(5-carboxypentyl)-2-((1E,3E)-5-((E)-1-(4-(1,3-dioxoisoindolin-2-yl)butyl)-3,3-dimethylindolin-2-ylidene)penta-1,3-dien-1-yl)-3,3-dimethyl-3H-indol-1-ium-5-sulfonate (2). As previously described [11]. ^{13}C NMR (850 MHz, CD_3OD) δ 177.22, 176.06, 169.94, 156.50, 155.18, 145.15, 143.30, 142.93, 142.83, 142.29, 135.45, 133.26, 129.82, 128.00, 127.25, 126.81, 124.18, 123.51, 121.29, 112.50, 111.15, 105.62, 104.21, 50.95, 50.19, 49.38, 44.75, 44.61, 40.40, 38.06, 34.60, 28.03, 27.95, 27.77, 27.34, 26.59, 25.72, 25.49. HRMS calculated $[M]^+$ for $C_{43}H_{47}N_3O_7S^+$ 750.3207, found 750.3214.

2.1.2.4. (E)-2-((2E,4E)-5-(1-(5-carboxypentyl)-3,3-dimethyl-3H-indol-1-ium-2-yl)penta-2,4-dien-1-ylidene)-1-(4-(1,3-dioxoisoindolin-2-yl)butyl)-3,3-dimethylindoline-5-sulfonate (3). As previously described [11]. ^{13}C NMR (850 MHz, CD_3OD) δ 177.22, 176.31, 169.93, 156.62, 155.00, 145.18, 143.33, 143.07, 142.71, 142.19, 135.45, 135.40, 133.29, 129.88, 127.98, 127.27, 126.95, 124.18, 124.09, 123.56, 121.28, 112.63, 111.03, 105.72, 104.15, 51.06, 50.08, 45.14, 44.23, 40.40, 38.09, 34.56, 34.45, 28.35, 28.30, 27.96, 27.75, 27.33, 27.26, 26.62, 25.69, 25.64, 25.19. HRMS calculated $[M]^+$ for $C_{43}H_{47}N_3O_7S^+$ 750.3207, found 750.3212.

2.1.2.5. 1-(5-carboxypentyl)-2-((1E,3E)-5-((E)-1-(4-(1,3-dioxoisoindolin-2-yl)butyl)-3,3-dimethyl-5-sulfonatoindolin-2-ylidene)penta-1,3-dien-1-yl)-3,3-dimethyl-3H-indol-1-ium-5-sulfonate (4). 1-(5-carboxypentyl)-2-((1*E*,3*E*)-5-((*E*)-1-(4-(1,3-dioxoisoindolin-2-yl)butyl)-3,3-dimethyl-5-sulfonatoindolin-2-ylidene)penta-1,3-dien-1-yl)-3,3-dimethyl-3*H*-indol-1-ium-5-sulfonate was obtained from 1-(5-carboxypentyl)-2,3,3-trimethyl-3*H*-indol-1-ium-5-sulfonate (1.7 g, 4.8 mmol), 1-(4-(1,3-dioxoisoindolin-2-yl)butyl)-2,3,3-trimethyl-3*H*-indol-1-ium-5-sulfonate (264.0 mg, 0.6 mmol), and *N*-((1*E*,3*E*)-3-(phenylimino)prop-1-en-1-yl) aniline hydrochloride (1.4 g, 5.3 mmol) in a 16% yield (86 mg) as a blue solid after lyophilisation. ^{1}H NMR (300 MHz, CD_3OD) δ 8.29 (dd, J = 12.2, 6.8 Hz, 2H), 7.93–7.75 (m, 8H), 7.37 (d, J = 8.4 Hz, 2H), 6.69 (t, J = 12.3 Hz, 1H), 6.36 (d, J = 13.6 Hz, 1H), 4.18 (d, J = 7.0 Hz, 4H), 3.76 (s, 2H), 2.36 (t, J = 7.2 Hz, 2H), 1.85 (s, 6H), 1.79–1.63 (m, 15H), 1.57–1.43 (m, 2H). ^{13}C NMR (850 MHz, CD_3OD) δ 175.61, 175.40, 175.10, 169.90, 156.25, 156.10, 144.92, 144.89, 143.40, 143.25, 142.65, 142.54, 135.62, 135.46, 135.41, 133.22, 132.87, 128.04, 128.02, 127.75, 124.16, 124.12, 124.08, 121.58, 121.34, 121.32, 111.76, 111.63, 50.59, 50.48, 45.03, 44.55, 40.39, 40.38, 38.07, 34.45, 28.11, 27.83, 27.22, 26.58, 25.65, 25.31, 24.50. HRMS calculated $[M+H]^+$ for $C_{43}H_{47}N_3O_{10}S_2^+$ 830.2736, found 830.2781.

2.1.2.6. 3-(5-carboxypentyl)-2-((1E,3E)-5-((E)-1-(4-(1,3-dioxoisoindolin-2-yl)butyl)-3,3-dimethylindolin-2-ylidene)penta-1,3-dien-1-yl)-1,1-dimethyl-1H-benzo[e]indol-3-ium (5). As previously described [11]. ^{13}C

NMR (850 MHz, CD_3OD) δ 176.56, 174.20, 169.96, 154.99, 154.97, 143.65, 142.57, 140.79, 135.41, 135.25, 133.47, 133.22, 131.76, 131.17, 129.77, 129.39, 128.75, 126.63, 126.18, 126.10, 124.12, 123.42, 123.36, 112.12, 111.91, 104.35, 104.08, 57.57, 57.47, 57.37, 52.56, 50.47, 44.71, 44.54, 38.10, 34.60, 31.12, 28.17, 27.99, 27.56, 27.39, 26.52, 25.74, 25.64, 17.20. HRMS calculated $[M]^+$ for $C_{47}H_{49}N_3O_4^+$ 719.3723, found 719.3734.

2.1.2.7. 1-(5-carboxypentyl)-2-((1E,3E,5E)-5-(3-(4-(1,3-dioxoisoindolin-2-yl)butyl)-1,1-dimethyl-1,3-dihydro-2H-benzo[e]indol-2-ylidene)penta-1,3-dien-1-yl)-3,3-dimethyl-3H-indol-1-ium (6). As previously described [11]. ^{13}C NMR (850 MHz, CD_3OD) δ 177.25, 176.71, 173.93, 169.95, 155.06, 154.83, 143.64, 142.45, 140.87, 135.45, 133.57, 133.30, 131.81, 131.15, 129.71, 129.42, 128.80, 126.63, 126.27, 125.97, 124.19, 123.40, 123.38, 112.20, 111.80, 104.44, 104.01, 57.67, 57.57, 57.47, 57.37, 57.27, 52.64, 50.36, 45.08, 44.17, 38.13, 34.58, 31.12, 28.55, 28.01, 27.54, 27.34, 26.64, 25.73, 25.34, 17.47, 17.38, 17.29, 17.20, 17.11. HRMS calculated $[M]^+$ for $C_{47}H_{49}N_3O_4^+$ 719.3723, found 719.3733.

2.1.2.8. 3-(5-carboxypentyl)-2-((1E,3E,5E)-5-(3-(4-(1,3-dioxoisoindolin-2-yl)butyl)-1,1-dimethyl-1,3-dihydro-2H-benzo[e]indol-2-ylidene)penta-1,3-dien-1-yl)-1,1-dimethyl-1H-benzo[e]indol-3-ium (7). 3-(5-carboxypentyl)-2-((1*E*,3*E*,5*E*)-5-(3-(4-(1,3-dioxoisoindolin-2-yl)butyl)-1,1-dimethyl-1,3-dihydro-2*H*-benzo[*e*]indol-2-ylidene)penta-1,3-dien-1-yl)-1,1-dimethyl-1*H*-benzo[*e*]indol-3-ium was obtained from 3-(5-carboxypentyl)-1,1,2-trimethyl-1*H*-benzo[*e*]indol-3-ium (2.4 g, 4.8 mmol), 3-(4-(1,3-dioxoisoindolin-2-yl)butyl)-1,1,2-trimethyl-1*H*-benzo[*e*] indol-3-ium (557.2 mg, 1.2 mmol), and *N*-((1*E*,3*E*)-3-(phenylimino) prop-1-en-1-yl)aniline hydrochloride (1.4 g, 5.28 mmol) in a 16% yield (150.0 mg) as a blue solid after lyophilisation. ^1H NMR (850 MHz, CD_3OD) δ 8.31 (q, $J = 13.1$ Hz, 2H), 8.23 (dd, $J = 23.6$, 8.4 Hz, 2H), 8.01 (dd, $J = 24.3$, 8.3 Hz, 2H), 7.94 (d, $J = 8.4$ Hz, 2H), 7.82–7.77 (m, 2H), 7.77–7.71 (m, 2H), 7.64 (p, 7.75 Hz, 2H), 7.59 (dd, $J = 22.0$, 8.6 Hz, 2H), 7.48 (dt, $J = 19.8$, 7.5 Hz, 2H), 6.64 (t, $J = 12.3$ Hz, 1H), 6.33 (d, $J = 13.6$ Hz, 1H), 4.26 (dt, $J = 15.3$, 7.0 Hz, 4H), 3.77 (t, $J = 6.4$ Hz, 2H), 2.34 (t, $J = 7.2$ Hz, 2H), 2.02 (s, 5H), 1.99 (s, 5H), 1.93–1.84 (m, 5H), 1.72 (p, $J = 7.65$ Hz, 2H), 1.58–1.53 (m, 2H), 1.22 (s, 4H). ^{13}C NMR (850 MHz, CD_3OD) δ 177.24, 176.03, 175.86, 169.94, 154.43, 154.37, 154.31, 154.26, 140.96, 140.88, 135.39, 135.15, 134.97, 133.46, 133.35, 133.20, 131.76, 131.70, 131.14, 129.45, 129.42, 128.76, 128.71, 126.58, 126.54, 126.14, 126.04, 124.11, 123.35, 123.31, 112.11, 112.04, 104.06, 103.98, 52.48, 52.39, 44.97, 44.43, 38.13, 34.60, 31.12, 28.50, 27.63, 27.61, 27.35, 26.54, 25.74, 25.63. HRMS calculated $[M]^+$ for $C_{51}H_{51}N_3O_4^+$ 770.3952, found 770.3989.

2.1.2.9. Synthesis of the hybrid tracer

2.1.2.9.1. c[RGDyK]. Synthesised as previously described [16].

2.1.2.9.2. DTPA(OtBu)$_4$-NHS. DTPA(*O-tert*-butyl ester)$_4$ (100.0 mg, 161.9 μmol), dipyrrolidino(*N*-succinimidyloxy)carbenium hexafluorophosphate (73.0 mg, 178.1 μmol) and DiPEA (141.0 μL, 809.3 μmol) were dissolved in DCM (5 mL, dried on 4 Å molecular sieves) and stirred for 15 h at r.t. The crude product was used without further purification in following reaction steps. HRMS calculated $[M]^+$ for $C_{34}H_{58}N_4O_{12}^+$ 715.4130, found 715.4193.

2.1.2.9.3. Phth-(SO$_3$)Cy5-c[RGDyK] (8). Compound **3** (20.0 mg, 26.7 μmol), dipyrrolidino(*N*-succinimidyloxy)carbenium hexafluorophosphate (12.0 mg, 29.3 μmol) and DiPEA (23.0 μL, 133.3 μmol) were dissolved in DMSO (400 μL). After stirring for 30 min at r.t., full conversion was confirmed by thin layer chromatography (TLC) and MALDI-TOF. c[RGDyK] (18.0 mg, 29.3 μmol) and DiPEA (9.3 μL, 53.0 μmol) were added and the solution was stirred at r.t. for 72 h whereafter TLC and MALDI-TOF indicated full consumption of c[RGDyK]. H_2O (0.1% v/v TFA) (2.4 mL) and CH_3CN (0.1% v/v TFA) (3 mL) were added and the compound was purified by reversed phase (RP)-HPLC and lyophilised, yielding a blue solid (10.0 mg, 28% isolated yield). ^1H NMR (850 MHz, CD_3OD) δ 8.28 (t, $J = 13.0$ Hz, 1H), 8.19 (t, $J = 13.0$ Hz, 1H), 7.86–7.83 (m, 3H), 7.82 (dd, $J = 8.2$, 1.6 Hz, 1H), 7.78 (dd, $J = 5.4$, 3.0 Hz, 2H), 7.54 (d, $J = 7.4$ Hz, 1H), 7.44 (t, $J = 7.7$ Hz, 1H), 7.37 (d, $J = 7.9$ Hz, 1H), 7.32 (t, $J = 7.4$ Hz, 1H), 7.28 (d, $J = 8.3$ Hz, 1H), 6.99 (d, $J = 8.5$ Hz, 2H), 6.67 (d, $J = 8.4$ Hz, 2H), 6.61 (t, $J = 12.3$ Hz, 1H), 6.39 (d, $J = 13.7$ Hz, 1H), 6.21 (d, $J = 13.3$ Hz, 1H), 5.21 (br. s, $J = 59.6$ Hz, 1H), 4.74 (t, $J = 7.0$ Hz, 1H), 4.40 (t, $J = 7.9$ Hz, 1H), 4.29–4.23 (m, 2H), 4.19 (t, $J = 7.4$ Hz, 2H), 4.11 (br. s, 2H), 3.90 (dd, $J = 10.9$, 3.8 Hz, 1H), 3.74 (br. s, $J = 6.1$ Hz, 2H), 3.57 (s, 1H), 3.39–3.37 (m, 1H), 3.34–3.32 (m, 1H), 3.28 (s, 1H), 3.23–3.21 (m, 1H), 3.21–3.17 (m, 1H), 3.15–3.10 (m, 1H), 3.06 (t, $J = 7.2$ Hz, 2H), 2.86 (d, $J = 7.9$ Hz, 2H), 2.80 (dd, $J = 16.4$, 7.6 Hz, 1H), 2.65 (s, 1H), 2.58 (dd, $J = 16.4$, 6.5 Hz, 1H), 2.21 (t, $J = 7.3$ Hz, 2H), 2.03 (s, 1H), 1.99 (s, 1H), 1.95 (d, $J = 11.7$ Hz, 1H), 1.90–1.78 (m, 7H), 1.74 (s, 6H), 1.72–1.60 (m, 10H), 1.56–1.51 (m, 1H), 1.51–1.44 (m, 3H), 1.44–1.38 (m, 1H), 1.38–1.29 (m, 2H), 1.28 (s, 1H), 1.21 (s, 1H), 1.12 (s, 1H), 1.11–1.07 (m, 1H), 1.00–0.92 (m, 1H). HRMS calculated $[M]^+$ $C_{70}H_{86}N_{12}O_{14}S^+$ 1350.6107, found 1350.6104.

2.1.2.9.4. NH$_2$-(SO$_3$)Cy5-c[RGDyK] (9). As described by Gromov *et al.* [30], *i.e.*, compound **8** (10.0 mg, 7.4 μmol) was dissolved in DMF (6 mL), and CH_3NH_2 (33 wt% in ethanol; EtOH; 20 mL) was added. After stirring at r.t. for 16 h, EtOH and CH_3NH_2 were removed *in vacuo* whereafter the product was redissolved in EtOH, precipitated in Et_2O (45 mL) and centrifuged subsequently. After decanting, the precipitate was washed with EtOAc (45 mL), centrifuged again and this was repeated twice with Et_2O (45 mL). The blue solid was desiccated, redissolved in H_2O/CH_3CN (4 mL; 1:1; 0.1% v/v TFA) and used directly in the following steps. HRMS calculated $[M]^+$ for $C_{62}H_{84}N_{12}O_{12}S^+$ 1220.6052, found 1220.6062.

2.1.2.9.5. DTPA-(SO3)Cy5-c[RGDyK] (10). Compound **9** (4.0 mg, 3.3 μmol) and DTPA(OtBu)$_4$-NHS (11.7 mg, 16.4 μmol) were dissolved in DMF (1.5 mL) followed by addition of DiPEA (5.7 μL, 32.7 μmol). The mixture was stirred for 4 h at r.t. until H_2O (0.1% v/v TFA) (2.5 mL) was added. The crude product was purified by RP-HPLC and lyophilised. To the resulting blue solid a 95:5 mixture of TFA/H_2O was added, resulting in a reddish solution which was shaken at r.t. for 2 h. Hereafter, the solvent was removed *in vacuo* and final purification was performed using RP-HPLC, yielding a blue solid (270.0 μg, 5% isolated yield) after lyophilisation. ^1H NMR (850 MHz, DMSO) δ 9.33–8.92 (m, 1H), 8.58–8.12 (m, $J = 65.6$, 35.6, 10.7 Hz, 3H), 7.87–7.75 (m, 1H), 7.74–7.57 (m, 2H), 7.42–7.32 (m, 2H), 7.30–7.21 (m, 2H), 7.04–6.86 (m, 2H), 6.80–6.53 (m, 10H), 4.66–4.51 (m, 1H), 4.47–4.36 (m, 1H), 4.36–4.29 (m, 1H), 4.26 (br s, 1H), 4.18 (s, 2H), 4.16–4.10 (m, 1H), 4.07–4.01 (m, 1H), 3.89 (dd, $J = 11.1$, 6.5 Hz, 1H), 3.68–3.59 (m, 2H), 3.51 (s, 2H), 3.46–3.42 (m, 5H), 2.99 (d, $J = 7.3$ Hz, 3H), 2.32–2.10 (m, 2H), 2.11–2.04 (m, 4H), 2.03–1.99 (m, 1H), 1.89 (s, 6H), 1.75 (s, 6H), 1.69 (s, 5H), 1.61 (s, 6H), 1.54–1.44 (m, 5H), 1.39 (dd, $J = 13.5$, 6.9 Hz, 2H), 1.35 (s, 2H), 1.23 (s, 2H), 1.15 (s, 4H), 1.05 (d, $J = 7.0$ Hz, 1H), 0.98 (d, $J = 7.5$ Hz, 1H), 0.92–0.76 (m, 4H). LRMS calculated $[M+H]^+$ for $C_{76}H_{107}N_{15}O_{21}S^+$ 1597.749, found 1597.766.

2.2. Stability towards glutathione

In an *in vivo* setting, interaction with the endogenous nucleophile glutathione can lead to unwanted adducts caused by cleavage. This experiment was performed based on previously published procedures [9], with the following deviations: 20 μL of the mixture was injected onto a Waters 1525 EF HPLC system using a SunFire C18 100 Å, 3.5 μm (150 × 4.6 mm) column and a gradient of 0.1% TFA in H_2O/0.1% TFA in CH_3CN 95:5 to 0.1% TFA in H_2O/0.1% TFA in CH_3CN 5:95 in 24 min. The mixture was then incubated at 37 °C for 6 h whereafter another 20 μL was injected for HPLC analysis. The stability of the fluorophores was calculated relative to the integration of the chromatogram at t = 0 h.

2.3. (Photo)physical properties

2.3.1. Lipophilicity

1-octanol (500 μL) was added to a 4 μM solution of either compound in phosphate-buffered saline (PBS; 500 μL) in a 2 mL Eppendorf tube (n = 6), or *vice versa*. The tubes were vortexed at maximum speed using an IKA Vibrofix VF1 (IKA®-Werke GmbH & Co. KG, Staufen, Germany) for 3 min and consecutively centrifuged for 5 min at 6000 × *g* in an Eppendorf 5415D centrifuge (Eppendorf, Hamburg, Germany). Hereafter, 100 μL of the organic phase as well as the aqueous phase was transferred to separate Eppendorf containers. To the organic phase, PBS (100 μL) was added followed by EtOH (200 μL). To the aqueous phase, 1-octanol (100 μL) and EtOH (200 μL) were added. Of each mixture (n = 12 per compound), 200 μL was transferred to a white Lumitrac 96-wells plate and fluorescence was measured whereafter the lipophilicity ($LogP_{o/w}$) was calculated.

2.3.2. Serum protein interaction

Serum protein interaction was measured (n = 3) as described previously [9] with the following deviations: The samples were incubated for 4 h and a control sample was included by adding compound to the reservoir chamber containing foetal calf serum (FCS).

2.3.3. Molar extinction coefficient (ε)

The molar extinction coefficient was assessed as described previously [9] with the following deviations: Stock solutions in DMSO-d_6 were diluted in DMSO, H_2O or PBS to obtain a concentration range of 7.5–0.25 μM. All optical densities were measured in 1 mL disposable plastic cuvettes (l = 1 cm; Brand, Germany).

2.3.4. Relative fluorescence quantum yield (Φ_F), Stokes shift and brightness

To determine the Φ_F, solutions in PBS were made for each fluorophore with a concentration where $A_{max} < 0.100$. Then, the absorbance at λ = 605 nm (**1**–**4**) λ = 630 nm (**6** and **5**), or λ = 640 nm (**7**) was measured. Fluorophores were excited at the abovementioned wavelengths to record fluorescence spectra. Dilutions were made by exchanging 500 μL of solution with PBS consequently, until at least 3 different concentrations were measured. The absorbance at the corresponding wavelength was then correlated to the sum of the fluorescence emission. The regression coefficient of the resulting plot was then compared to the regression coefficient of a suitable, known reference compound (either **Methyl-(SO_3)Cy5-COOH, EuK-Cy5(Ar)-mas$_3$**, or **sulfonate-(Ar)Cy5(Ar)-COOH**; Φ_F = 13% [9], 12% [11], and 10% [13], respectively). The Stokes shift was determined using the $\lambda_{ex,max}/\lambda_{em,max}$ values of the recorded spectra. The brightness of the fluorophores was calculated by multiplying the corresponding molar extinction coefficient (ε) with the corresponding quantum yield (Φ_F). The brightness of **10** was determined by using the molar extinction coefficient of the corresponding unconjugated fluorophore.

2.3.5. Stacking behaviour

These values were determined as described previously [9], with the following deviations: DMSO stock solutions of each fluorophore were diluted to concentrations ranging between 0.78–50 μM.

2.4. Photostability

The photostability assay was carried out based on previously reported methods [13], with the following deviations: the cuvettes were placed at a 5 cm distance in front of a prototype Karl Storz camera setup (Karl Storz Endoskope GmbH & Co. KG, Tuttlingen, Germany). This camera setup included an IMAGE1 S H3-Z FI Three-Chip FULL HD camera head equipped with a 0° laparoscope in combination with an IMAGE 1 S CONNECT module, an IMAGE 1 S H3-LINK link module and a Cy5-modified D-light C light source (590–680 nm emission). A standard eyepiece adapter containing a bandpass filter (640–720 nm; Cat no. 20100034; Karl Storz Endoskope GmbH & Co. KG) was placed between the camera and the laparoscope to image the Cy5 fluorescence. The sum of the fluorescence emission was plotted for each fluorophore at the different time points. It must be noted that the time required for direct illumination during surgical resection is well below the 30-min direct, constant illumination timeframe used in the current setup.

As a control for solubility issues, the most hydrophobic compound **7** was measured without irradiation by the Storz camera while all other variables in the setup were kept at the same level.

2.5. Signal penetration depth

The signal penetration depth was carried out as described by van Willigen *et al.* [25], with the following deviations: all fluorophores were dissolved in H_2O and supplemented with human serum albumin and the point at which the capillaries became indistinguishable from diffused light was determined by three independent observers.

2.6. Flow cytometry

Receptor affinity (k_D) of the hybrid tracer for the $\alpha_v\beta_3$ integrin was measured in saturation experiments using Geβ3 cells as previously published [22]. Normalized geometric means were fitted with equations in the GraphPad Prism 7 software. The k_D values were calculated using the "Binding–Saturation, One site–Total" nonlinear regression equation (eq (1)), with the background value set at 0.

$$\log IC_{50} = \log\left(10^{\log K_D}\left(1 + \frac{[ref]}{K_{D,\,ref}}\right)\right) \quad (1)$$

2.7. Radiolabelling, in vivo tumour model, and biodistribution

Radiolabelling of **10** and the reference tracer **11** with ^{111}In, the development of the orthotopic 4T1 breast tumour model in nude BALB/c mice, and biodistribution experiments were carried out according to previously described procedures [22]. The local ethics committee of the Leiden University Medical Center (LUMC) approved all animal experiments prior to execution. Experiments were performed in accordance with the Experiments on Animals Act (Wod, 2014) and the applicable legislation in the Netherlands in accordance with the European guidelines (EU directive no. 2010/63/EU) regarding the protection of animals used for scientific purposes. Mice were kept in accordance to the Dutch law in a licensed establishment for use of experimental animals (animal facility of the LUMC).

3. Results

3.1. Synthesis

All fluorophores were synthesised following the procedures as previously described [11]. The asymmetrical orthogonal **2** could readily be conjugated to DTPA and c[RGDyK] after liberating the amine, yielding the tracer **10** (Scheme 2). Subsequent radiolabelling of this tracer with $^{111}InCl_3$ then yielded the hybrid tracer **^{111}In-10**.

3.2. Chemical stability

No differences in chemical stability towards glutathione (≥ 88%) dependent on the substitution pattern were seen between the different fluorophore analogues. These findings are in line with previous reports on the stability of cyanine fluorophores (*i.e.*, cyanine fluorophores without an aryl ether bond in the polymethine chain) towards glutathione [9,13]. **7** was excluded from this comparison as its low polarity gave rise to solubility issues at the required concentration.

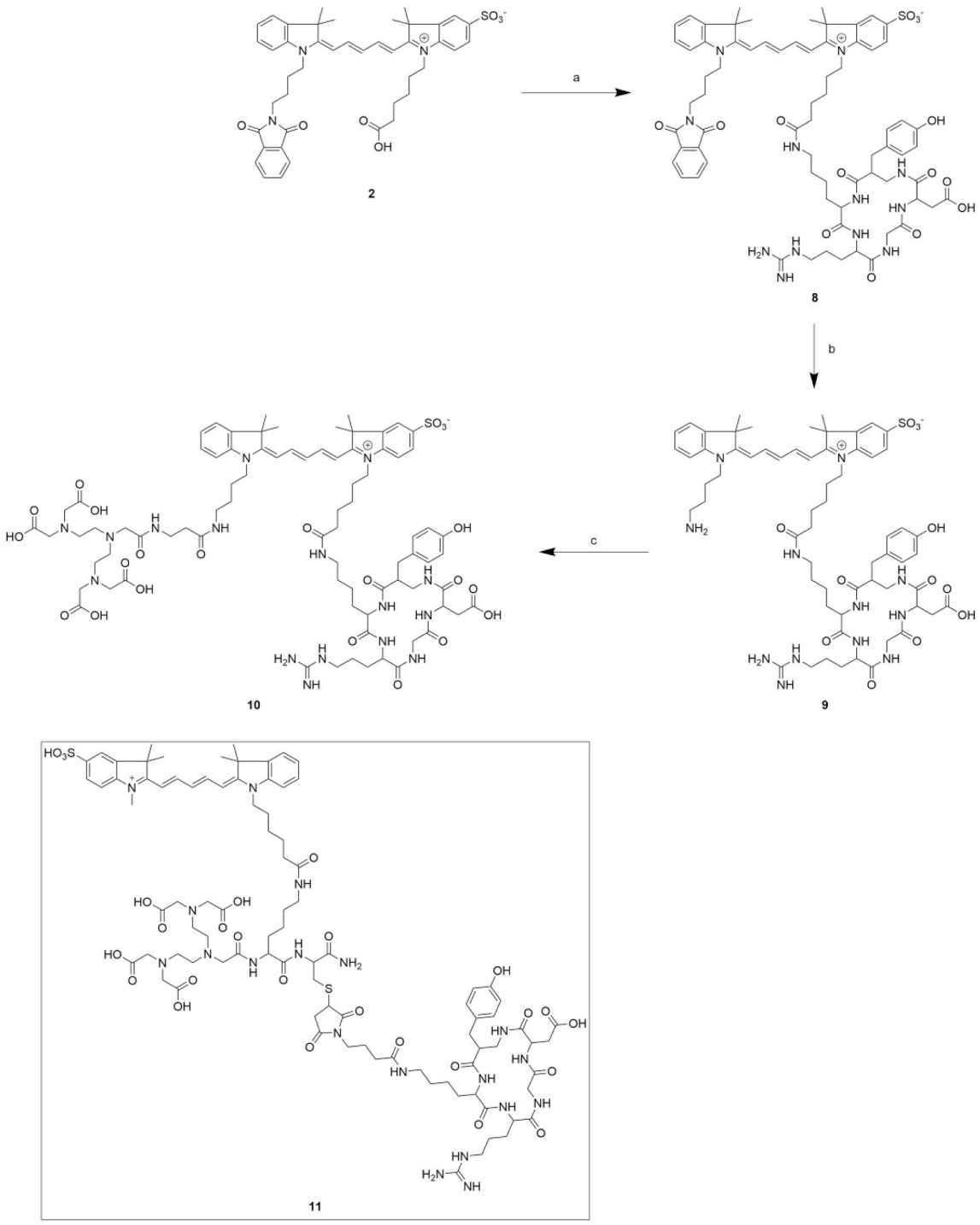

Scheme 2. Synthetic strategy for **10**, a hybrid tracer based on the design by using a fluorophore as linker. a) i) HSPyU, DiPEA, DMSO, r.t., 30 min, ii) c[RGDyK], DiPEA r.t., 72 h; b) CH_3NH_2 (33 wt% in EtOH), DMF, 4 h, r.t.; c) (i) DTPA(OtBu)$_4$-NHS, DMF, DiPEA, r.t., 4 h; (ii) TFA/H_2O (95:5), r.t., 2 h.

3.3. Lipophilicity and serum binding

The partition coefficient in octanol/water ($LogP_{(o/w)}$) of the cyanine fluorophores was statistically significantly lowered by addition of sulfonates and increased by the addition of an extra benzene moiety ($p < 0.005$, Table 1), which is in line with previously published results [31]. Interestingly, the addition of two benzene moieties (resulting in **7**) did not necessarily influence the $LogP_{(o/w)}$ of the cyanine fluorophore to a statistically significant degree ($p < 0.05$, Table 1), indicating a limitation to this extension.

Serum binding was influenced to some extent by molecular

Table 1
Lipophilicity ($LogP_{(o/w)}$) and serum binding.

Compound	$LogP_{(o/w)}$ (n = 6)	Serum binding (% bound, n = 3)
1	1.13 ± 0.07	93.8 ± 1.3
2	0.01 ± 0.01	87.1 ± 0.3
3	−0.04 ± 0.01	84.5 ± 0.3
4	−1.56 ± 0.01	67.3 ± 2.7
5	1.05 ± 0.01	92.8 ± 0.9
6	1.23 ± 0.04	92.7 ± 0.8
7	1.17 ± 0.03	88.0 ± 1.7

alterations (Table 1). The addition of one or more sulfonate(s) statistically significantly decreased the serum binding ($p \leq 0.0006$), whereas the addition of one benzene moiety was shown to induce no changes ($p > 0.05$). However, statistically significant changes were found when comparing **7** (88.0 ± 1.7%) to **1** (93.8 ± 1.3%; $p = 0.0026$). An indication was found that some correlation between the lipophilicity and serum binding exists, *i.e.*, the serum binding of a fluorophore increases as its lipophilicity of increases ($r = 0.8975$, $p = 0.0012$; $r^2 = 0.8818$; Figure SI22).

3.4. Photophysical properties

Addition of sulfonate or benzene moieties can result in alterations to the (photo)physical properties of the Cy5 fluorophore. The differences found in brightness, photostability and stacking behaviour are reported below.

3.4.1. Brightness

All studied fluorophores exhibited a higher ε in DMSO than in H_2O and PBS (Table 2). The ε of the sulfonated Cy5 fluorophores was shown to be clearly related to the site and number of substitutions (**4** > **3** > **1** > **1**; Table 2). In concurrence with previous reports [9], the addition of one sulfonate at the C5 position of the carboxylic-acid-containing indole moiety diminished the ε, while the addition of a sulfonate moiety at the C5 position of the phthalimide-containing indole moiety caused an increase in the ε; a trend that seems inapplicable to the benzo[*e*]indole--containing fluorophores (Table 2). Interestingly, the addition of a sulfonate on the phthalimide-bearing indole increased the ε to a larger extent than a sulfonate on the carboxylic-acid-bearing indole. This finding was unexpected, as the phthalimide does not participate in the conjugated system of the cyanine as it is separated from this system by four methylenes.

The Φ_F of sulfonated Cy5 fluorophores **2**–**4** was higher than the Cy5 fluorophore without C5 indole substitutions **1** and the benzo[*e*]indole-containing Cy5 fluorophores **5**–**7** (Table 2). These data resulted in the following trend in brightness: **4** ≫ **3** > **2** > **1** > **6** > **7** > **5** (Table 2).

3.4.2. Photostability

The performed experiments indicated that the addition of sulfonates increased the photostability, but this effect was not dependent on the amount of sulfonates (**1** < **3** ≈ **2** ≈ **4**; $p < 0.05$; Table 2). The photostability of the benzo[*e*]indole-containing cyanine fluorophores was lower and dependent on the degree of functionalization (**1** > **6** ≈ **5** > **7**; $p < 0.05$ Table 2).

3.4.3. Stacking behaviour

When the presented fluorophores were analysed for their stacking behaviour, it was found that the incorporation of benzo[*e*]indole moieties drove both H- and J-stacking (*i.e.*, a sandwich-type or brickstone arrangement, respectively) [32] in both H_2O and PBS (Fig. 1). Here it seems that the planar and hydrophobic nature of these fluorophores (see Table 1, $LogP_{(o/w)}$), drives the van der Waal's forces that cause formation of H- or J-aggregates [13]. Conversely, the introduction of a single (tetrahedral) sulfonate moiety on either indole decreased H- and J-stacking (Fig. 1) as a result of Coulombic repulsion [32].

3.5. Signal penetration depth in porcine tissue

The fluorescence penetration depth was measured in porcine tissue using a clinical grade STORZ laparoscopic camera and compared to the brightness of the corresponding fluorophore. In concordance with previously published results [25], all fluorophores were visible up to about 7 mm of layers of tissue (except for **6**, approximately 4 mm; Figure SI23). No clear correlation between the brightness of a fluorophore and its tissue penetration could be established.

3.6. In vitro and in vivo evaluation of fluorophore performance in a hybrid tracer

2 was selected as this fluorophore structure has proven to be most favourable in a previous study on end-labelled Cy5 fluorophores [16]. Flow cytometry experiments revealed an affinity for $\alpha_v\beta_3$ integrin in Geβ3 cells of $k_D = 34.1 \pm 13.3$ nM (Figure SI24) for **10**, which is comparable to the reference compound **11**; $k_D = 30.3 \pm 5.7$ nM) [16].

The biodistribution data (Fig. 2) show that the uptake in tumorous tissue as well as non-targeted tissue for **10** is significantly higher after 2 h than the uptake for **11**. Only blood uptake (0.065 ± 0.034 %ID/g for **10** *vs.* 0.034 ± 0.0064 %ID/g for **11**; $p > 0.05$) after 2 h showed statistically nonsignificant changes between the two tracers. These data imply that the tracer is cleared not only through the renal clearance pathway, but also through the hepatobiliary pathway and that the clearance rate for **10** is much slower compared to **11**.

4. Discussion

By creating seven structurally different asymmetrical Cy5 fluorophores (Scheme 1), the influences that substituents at the (C4 and) C5 position on either (or both) indole(s) have on several (photo)physical properties (*i.e.*, lipophilicity, serum protein binding, molar extinction coefficient (ε), fluorescence quantum yield, stacking behaviour,

Table 2
Photophysical properties of Cy5 fluorophores and hybrid tracer analogues.

Compound	Molar extinction coefficient (ε; · 10^5 M^{-1} cm^{-1})			$\lambda_{ex,max}/\lambda_{em,max}$ (Stokes shift; nm)			Φ_F (%)	Brightness (· 10^3 M^{-1} cm^{-1})	Photostability (% remaining fluorescence, n = 4)
	DMSO	H_2O	PBS	DMSO	H_2O	PBS	PBS	PBS	
1	1.86	0.92	0.93 [11]	650/670 (20)	644/656 (12)	644/660 (16)	4	3.72	70.1 ± 6.0
2	1.36	0.82	0.95 [11]	655/676 (21)	646/663 (17)	646/664 (18)	6	5.70	85.0 ± 2.1
3	2.23	1.29	1.46 [11]	655/674 (19)	643/662 (19)	643/662 (19)	6	8.76	86.2 ± 4.3
4	3.06	2.60	2.86	660/680 (20)	649/666 (17)	649/666 (17)	15	42.9	90.6 ± 3.7
5	1.78	0.46	0.37 [11]	670/691 (21)	669/677 (8)[a]	662/680 (18)	2	0.74	57.7 ± 2.4
6	1.89	0.43	0.60 [11]	670/692 (22)	663/691 (28)[a]	662/679 (17)	4	2.40	53.8 ± 4.6
7	1.81	0.27	0.50	689/710 (21)	n.d.[b]	n.d.[b]	4	2.00	24.4 ± 5.6

[a] measurements influenced by poor solubility.
[b] could not be measured due to poor solubility.

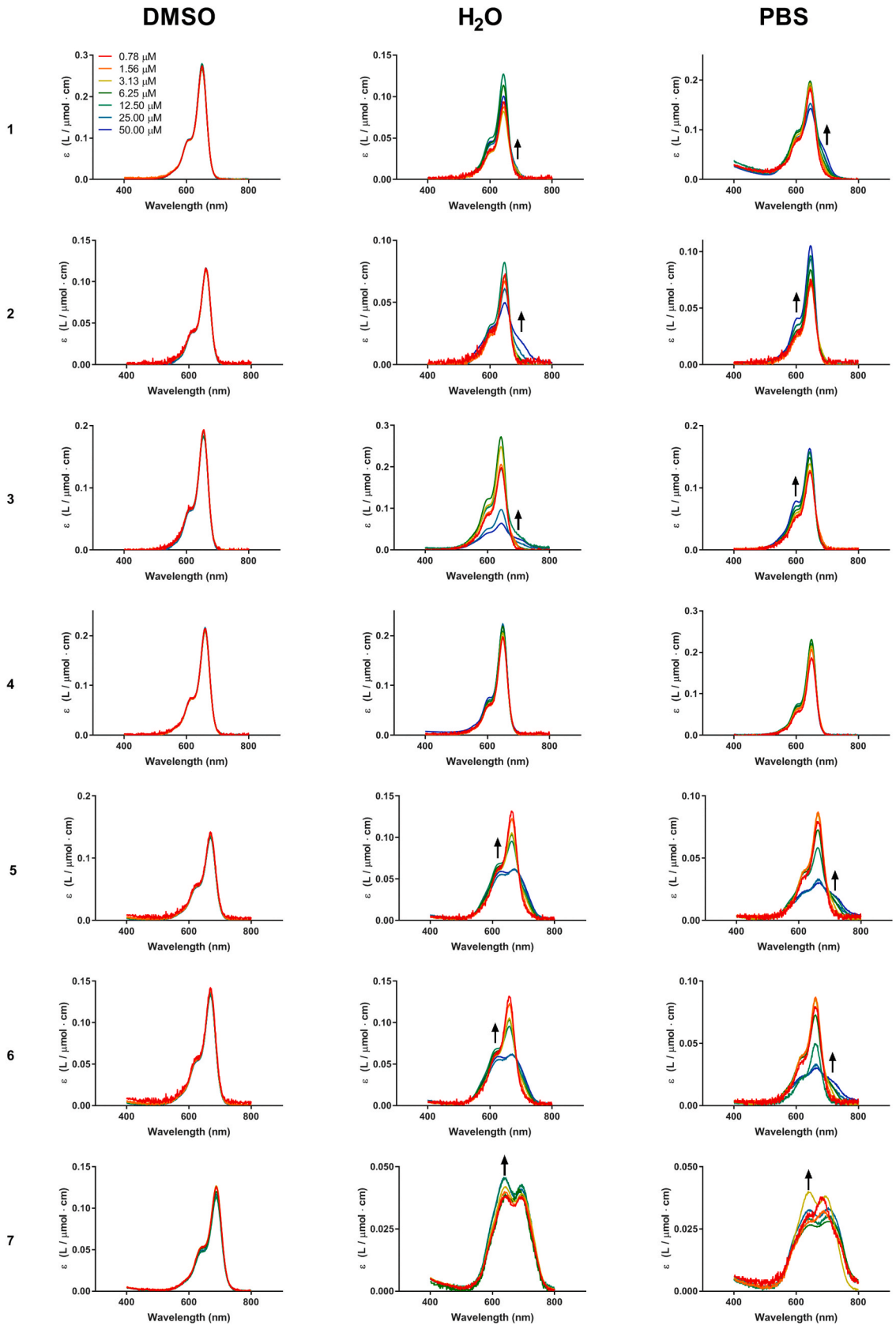

Fig. 1. Stacking behaviour of **1**–**7** in different solvents. Stacking of the individual fluorophores was measured at different concentrations (0.78–50 μM) in DMSO, H_2O and PBS. Data show severe stacking for all benzene- and unsubstituted fluorophores in H_2O and PBS. Arrows indicate change in absorbance intensity between spectra.

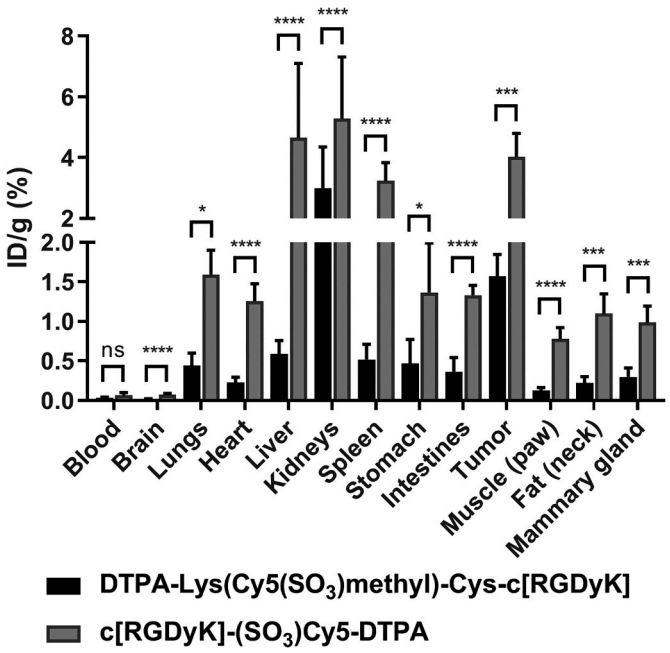

Fig. 2. Biodistribution data of the hybrid tracer **10** *vs.* a reference compound **11** [16].

chemical- and photostability, and penetration depth in porcine tissue) of cyanine fluorophores could be mapped.

Prior to these findings, it was Fisher *et al.* [8] and Spa *et al.* [9] who indicated that no clear trend between cyanine substitution pattern on the indoles and Φ_F could be established, but the data presented here suggest otherwise; *i.e.*, sulfonates were shown to increase the Φ_F of a fluorophore whereas extra benzene moieties diminished the Φ_F (Table 2). Stacking can affect the photophysical characteristics of a fluorophore in aqueous media, *e.g.*, induce a batho- or hypsochromic shift or greatly diminish the brightness of a fluorophore. The cyanine core (without C5-indole substitutions) is prone to fluorophore–-fluorophore stacking [33,34] as its molecular structure is relatively planar. The fluorophore–fluorophore aggregation was diminished by the addition of sulfonates, yet increased by the addition of extra benzene rings, correlating to the solubility of these compounds in aqueous media. The latter, however, is also dependent on moieties conjugated on the *N*-indole position. Interestingly, the variations in brightness only revealed a small variation in the in-depth tissue penetration of the different fluorophore. Overall, **4** had shown to possess the most favourable photophysical properties and that the addition of benzene moieties on the cyanine backbone diminishes the ε, Φ_F, and thereby the brightness.

Another trend between the substitution pattern and a (photo) physical characteristic was found in photobleaching. Fluorophores typically undergo photobleaching upon exposure to a bright light source. This process, where the molecular structure of the fluorophores is disintegrated, causes a loss in fluorescence signal intensity [35,36]. The results imply that the addition of one (or more) sulfonate (s) (compound **2**–**4**) statistically significantly increases the photophysical stability of the fluorophore when comparing to the unsubstituted fluorophore **1** (Table 2, $p < 0.05$), whereas benzo[*e*] indole-containing analogues (compound **5**–**7**) statistically significantly decrease the photostability of the fluorophore (Table 2, $p < 0.05$). This trend is in line with previously published results [9,13] and suggests that benzo[*e*]indole-containing cyanine fluorophores need sulfonate substituents to compensate their reduced photostability. Uniquely, a synthesised fluorophore could function as a bifunctional linker after liberation of the amine. This ability to functionalise both the carboxylic acid and the primary amine in an orthogonal manner allows for new possibilities in fluorescent and hybrid tracer design. Previous reports on $\alpha_v\beta_3$-targeted molecular imaging indicated that end-labelled fluorophores with one sulfonate yielded the most favourable properties when conjugated to a targeting vector [16]. In this study, *in vitro* and *in vivo* evaluation of the hybrid tracer **10** showed that the fluorophore could function as a scaffold when conjugated to both c[RGDyK] and DTPA in an orthogonal fashion. These experiments, however, also illustrate that the favourable fluorophore–receptor interaction observed with our prostate-specific-membrane-antigen-targeted hybrid tracers [11] did not translate directly to $\alpha_v\beta_3$. This finding implies that the properties of the targeting vector should dictate the use of specific fluorophores, be it in an end-labelled or linker fashion.

As a result of these studies, we hope to aid chemists in their scrutiny for the optimisation of fluorescent and/or hybrid targeted tracers and as such, achieve better patient care.

5. Conclusion

The influence of structural alterations of an indole moiety at the (C4 and) C5 position on selected properties of Cy5 fluorophores has been evaluated. By doing so, it could be concluded that sulfonates are generally favourable for the photophysical properties of a fluorophore, whereas extra benzene rings bring about disadvantageous characteristics. Furthermore, it has been shown that with the availability of (a) symmetrical orthogonal Cy5 fluorophores, a door has been opened for new and innovative tracer designs and synthetic strategies.

CRediT authorship contribution statement

Albertus W. Hensbergen: Investigation, Formal analysis, Writing - original draft. **Mathijs A.C. de Kleer:** Investigation, Writing - review & editing. **Michael S. Boutkan:** Investigation, Writing - review & editing. **Danny M. van Willigen:** Investigation, Writing - review & editing. **Felicia A. van der Wijk:** Investigation, Writing - review & editing. **Mick M. Welling:** Investigation, Writing - review & editing. **Hans-Jürgen Wester:** Conceptualization, Writing - review & editing. **Tessa Buckle:** Investigation, Writing - review & editing. **Fijs W.B. van Leeuwen:** Conceptualization, Supervision, Writing - review & editing, Funding acquisition.

Declaration of competing interest

The authors declare that they have no known competing financial interests or personal relationships that could have appeared to influence the work reported in this paper.

Acknowledgements

This research was funded by an NWO-TTW-VICI grant (TTW 16141). The authors thank Dr. Jan Wouter Drijfhout for the use of, and assistance with instruments, Bjorn van Doodewaerd for support regarding HRMS measurements and Dr. Karthick Sai Sankar Gupta for support regarding NMR measurements.

Appendix A. Supplementary data

Supplementary data to this article can be found online at https://doi.org/10.1016/j.dyepig.2020.108712.

References

[1] Alander JT, Kaartinen I, Laakso A, Patila T, Spillmann T, Tuchin VV, et al. A review of indocyanine green fluorescent imaging in surgery. Int J Biomed Imag 2012; 2012:940585.
[2] Marmor MF, Ravin JG. Fluorescein angiography: insight and serendipity a half century ago. Arch Ophthalmol 2011;129(7):943–8.

[3] Burggraaf J, Kamerling IM, Gordon PB, Schrier L, de Kam ML, Kales AJ, et al. Detection of colorectal polyps in humans using an intravenously administered fluorescent peptide targeted against c-Met. Nat Med 2015;21(8):955–61.
[4] VEGF-targeted fluorescent tracer imaging in breast cancer.
[5] Interest of fluorescence in salvage surgery for recurrence of head and neck cancer in irradiated area. 2012.
[6] Lavis LD, Raines RT. Bright ideas for chemical biology. ACS Chem Biol 2008;3(3):142–55.
[7] Widengren J, Schwille P. Characterization of photoinduced isomerization and back-isomerization of the cyanine dye Cy5 by fluorescence correlation spectroscopy. J Phys Chem 2000;104(27):6416–28.
[8] Fisher NI, Hamer FM, Pope WJ. A comparison of the absorption spectra of some typical symmetrical cyanine dyes. Proceedings of the Royal Society of London Series A - Mathematical and Physical Sciences 1997;154(883):703–23.
[9] Spa SJ, Hensbergen AW, van der Wal S, Kuil J, van Leeuwen FWB. The influence of systematic structure alterations on the photophysical properties and conjugation characteristics of asymmetric cyanine 5 dyes. Dyes Pigments 2018;152:19–28.
[10] Buckle T, van Willigen DM, Spa SJ, Hensbergen AW, van der Wal S, de Korne CM, et al. Tracers for fluorescence-guided surgery: how elongation of the polymethine chain in cyanine dyes alters the pharmacokinetics of a dual-modality c[RGDyK] tracer. J Nucl Med 2018;59(6):986–92.
[11] Hensbergen AW, Buckle T, van Willigen DM, Schottelius M, Welling MM, van der Wijk FA, et al. Hybrid tracers based on cyanine backbones targeting prostate-specific membrane antigen: tuning pharmacokinetic properties and exploring dye-protein interaction. J Nucl Med 2020;61(2):234–41.
[12] Schwechheimer C, Ronicke F, Schepers U, Wagenknecht HA. A new structure-activity relationship for cyanine dyes to improve photostability and fluorescence properties for live cell imaging. Chem Sci 2018;9(31):6557–63.
[13] van der Wal S, Kuil J, Valentijn ARPM, van Leeuwen FWB. Synthesis and systematic evaluation of symmetric sulfonated centrally C C bonded cyanine near-infrared dyes for protein labelling. Dyes Pigments 2016;132:7–19.
[14] Choi HS, Nasr K, Alyabyev S, Feith D, Lee JH, Kim SH, et al. Synthesis and in vivo fate of zwitterionic near-infrared fluorophores. Angew Chem Int Ed Engl 2011;50(28):6258–63.
[15] Lee H, Mason JC, Achilefu S. Heptamethine cyanine dyes with a robust C-C bond at the central position of the chromophore. J Org Chem 2006;71(20):7862–5.
[16] Bunschoten A, van Willigen DM, Buckle T, van den Berg NS, Welling MM, Spa SJ, et al. Tailoring fluorescent dyes to optimize a hybrid RGD-tracer. Bioconjugate Chem 2016;27(5):1253–8.
[17] Kuil J, Buckle T, Oldenburg J, Yuan H, Borowsky AD, Josephson L, et al. Hybrid peptide dendrimers for imaging of chemokine receptor 4 (CXCR4) expression. Mol Pharm 2011;8(6):2444–53.
[18] Tan X, Luo S, Wang D, Su Y, Cheng T, Shi C. A NIR heptamethine dye with intrinsic cancer targeting, imaging and photosensitizing properties. Biomaterials 2012;33(7):2230–9.
[19] Komljenovic D, Wiessler M, Waldeck W, Ehemann V, Pipkorn R, Schrenk HH, et al. NIR-cyanine dye linker: a promising candidate for isochronic fluorescence imaging in molecular cancer diagnostics and therapy monitoring. Theranostics 2016;6(1):131–41.
[20] Dost TL, Gressel MT, Henary M. Synthesis and optical properties of pentamethine cyanine dyes with carboxylic acid moieties. Anal Chem Insights 2017;12.1177390117711938.
[21] van der Wal S, de Korne CM, Sand LGL, van Willigen DM, Hogendoorn PCW, Szuhai K, et al. Bioorthogonally applicable fluorescence deactivation strategy for receptor kinetics study and theranostic pretargeting approaches. Chembiochem 2018;19(16):1758–65.
[22] Hensbergen AW, van Willigen DM, Welling MM, van der Wijk FA, de Korne CM, van Oosterom MN, et al. Click chemistry in the design and production of hybrid tracers. ACS Omega 2019;4(7):12438–48.
[23] Kelderhouse LE, Chelvam V, Wayua C, Mahalingam S, Poh S, Kularatne SA, et al. Development of tumor-targeted near infrared probes for fluorescence guided surgery. Bioconjugate Chem 2013;24(6):1075–80.
[24] Chen Y, Pullambhatla M, Banerjee SR, Byun Y, Stathis M, Rojas C, et al. Synthesis and biological evaluation of low molecular weight fluorescent imaging agents for the prostate-specific membrane antigen. Bioconjugate Chem 2012;23(12):2377–85.
[25] van Willigen DM, van den Berg NS, Buckle T, KleinJan GH, Hardwick JC, van der Poel HG, et al. Multispectral fluorescence guided surgery; a feasibility study in a phantom using a clinical-grade laparoscopic camera system. Am J Nucl Med Mol Imaging 2017;7(3):138–47.
[26] Haubner R, Wester HJ. Radiolabeled tracers for imaging of tumor angiogenesis and evaluation of anti-angiogenic therapies. Curr Pharmaceut Des 2004;10(13):1439–55.
[27] Kapp TG, Rechenmacher F, Neubauer S, Maltsev OV, Cavalcanti-Adam EA, Zarka R, et al. A comprehensive evaluation of the activity and selectivity profile of ligands for RGD-binding integrins. Sci Rep 2017;7:39805.
[28] Pedersen D, Rosenbohm C. Dry column vacuum chromatography. Synthesis 2004;2001(16):2431–4.
[29] Lopalco M, Koini EN, Cho JK, Bradley M. Catch and release microwave mediated synthesis of cyanine dyes. Org Biomol Chem 2009;7(5):856–9.
[30] Gromov SP, Fomina MV, Nikiforov AS, Vedernikov AI, Kuz'mina LG, Howard JAK. Synthesis of symmetrical cyanine dyes with two N-ammonioalkyl groups. Tetrahedron 2013;69(29):5898–907.
[31] Mujumdar RB, Ernst LA, Mujumdar SR, Lewis CJ, Waggoner AS. Cyanine dye labeling reagents: sulfoindocyanine succinimidyl esters. Bioconjugate Chem 1993;4(2):105–11.
[32] Kobayashi T. J-Aggregates, vol. 1. World Scientific; 1996. p. 1–40.
[33] Levitus M, Ranjit S. Cyanine dyes in biophysical research: the photophysics of polymethine fluorescent dyes in biomolecular environments. Q Rev Biophys 2011;44(1):123–51.
[34] Landsman ML, Kwant G, Mook GA, Zijlstra WG. Light-absorbing properties, stability, and spectral stabilization of indocyanine green. J Appl Physiol 1976;40(4):575–83.
[35] Kim S, Lim YT, Soltesz EG, De Grand AM, Lee J, Nakayama A, et al. Near-infrared fluorescent type II quantum dots for sentinel lymph node mapping. Nat Biotechnol 2004;22(1):93–7.
[36] Nakayama A, Bianco AC, Zhang CY, Lowell BB, Frangioni JV. Quantitation of brown adipose tissue perfusion in transgenic mice using near-infrared fluorescence imaging. Mol Imag 2003;2(1):37–49.